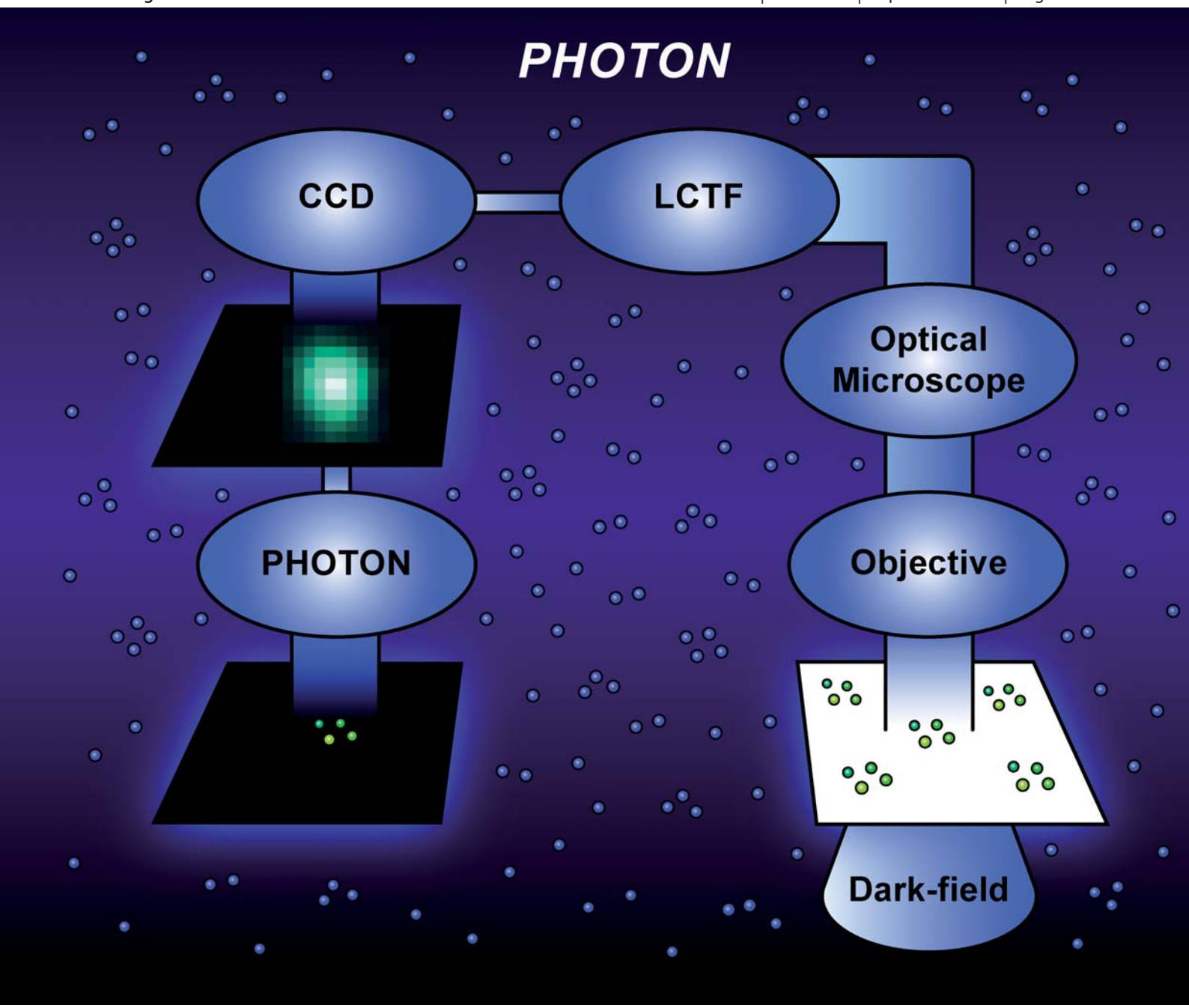
Nanoscale

www.rsc.org/nanoscale

Volume 3 | Number 9 | September 2011 | Pages 3411–3942



ISSN 2040-3364

COVER ARTICLE

Huang and Xu
Multicolored nanometre-resolution mapping of single protein–ligand binding complexes using far-field photostable optical nanoscopy (PHOTON)

RSC Publishing

NCNST

2040-3364(2011)3:9;1-J

Nanoscale

Dynamic Article Links

Cite this: *Nanoscale*, 2011, **3**, 3567

www.rsc.org/nanoscale

COMMUNICATION

Multicolored nanometre-resolution mapping of single protein–ligand binding complexes using far-field photostable optical nanoscopy (PHOTON)†

Tao Huang and Xiao-Hong Nancy Xu*

Received 17th February 2011, Accepted 10th May 2011
DOI: 10.1039/c1nr10182j

Mapping of individual ligand molecules and their binding sites in single protein–ligand complexes at nanometer resolution in real-time would enable probing their structures and functions *in vitro* and *in vivo*. In this study, we have developed far-field *phot*ostable *o*ptical *n*anoscopy (PHOTON) for mapping single ligand molecules (biotin) and their binding sites in individual protein–ligand complexes (streptavidin–biotin) with 1.2 nm spatial resolution and 100 ms temporal resolution. PHOTON includes one standard far-field optical microscope with a halogen-lamp illuminator; single-molecule-nanoparticle-optical-biosensors (SMNOBS) with exceptionally high quantum-yield (QY) of Rayleigh scattering and photostability (non-photobleaching, non-photoblinking) as imaging probes; and Multispectral Imaging System (MSIS) for spectral isolation of individual SMNOBS with 1 nm wavelength resolution. Intrinsic size- and shape- dependent localized-surface-plasmon-resonance (LSPR) spectra of single SMNOBS provide multiple-spectral (color) nanoprobes for sub-diffraction imaging, offering feasibility of probing of binding structures and functions of single protein–ligand complexes at nm (potentially achieving Ångstrom) resolution in real-time.

Far-field optical microscopy possesses extraordinary versatility for imaging of biomolecules and living organisms in their native environments in real time. In comparison with scanning probe microscopy (*e.g.*, near-field optical microscopy or atomic force scanning microscopy), optical microscopy is able to image larger area and numerous molecules of interest rapidly and simultaneously. Optical microscopy is also able to image intracellular dynamic events of single living organisms in real time. Such distinctive capabilities enable the study of molecular interactions and intracellular dynamic events (*e.g.*, signaling transduction pathways) with remarkably rapid temporal resolution.

Unfortunately, its spatial resolution is conventionally limited by optical diffraction (~250 nm).[1] However, far-field optical microscopy can potentially achieve spatial resolution far beyond optical diffraction limit, if sufficient amount of photons (N) from an object are collected, as described in eqn (1).[2,3]

$$\sigma = \sqrt{\frac{S^2}{N} + \frac{a^2}{12N} + \frac{8\pi S^4 b^2}{a^2 N^2}} \quad (1)$$

where σ is uncertainty of centroid (position) of an object; S is standard deviation of the point spread function (PSF); a is the pixel size of an imaging detector; b is the standard deviation of background noise; and N is the number of collected photons.

Recently, far-field fluorescence microscopy has achieved sub-diffraction resolution by isolating single fluorescence molecules.[4] Typically, fluorophore molecules were repeatedly photobleached and reactivated for multiple cycles, leading to intrinsic slow temporal resolution. Notably, fluorescence microscopy uses fluorophores as probes. Single fluorophores or quantum dots (QDs) suffer photobleaching and photoblinking, which limits their applications in imaging of dynamic events of interest for any desired period of time. They also require single-wavelength excitation sources (*e.g.*, lasers), which create auto-fluorescence of proteins and phototoxicity toward living organisms.[4,5] These well-known fundamental limitations demand development of new photostable optical imaging probes and tools.

In this study, we have developed a new-generation sub-diffraction imaging nanoscope (PHOTON), which uses a standard far-field optical microscope equipped with a multi-spectral imaging system (MSIS) (Fig. 1). The illumination source is a standard microscopic white-light illuminator (100 W halogen lamp). No laser excitation source is needed. Thus, a conventional optical microscope is well suited for super-resolution imaging. Unlike fluorescence microscopy, PHOTON uses Rayleigh scattering of single noble metal nanoparticles (*e.g.*, Ag NPs) as optical probes, overcoming the drawbacks (auto-fluorescence, photobleaching, phototoxicity) of fluorescence-based microscopy for imaging of proteins and living organisms.

Notably, plasmonic optical properties of single noble metal NPs (*e.g.*, Ag NPs) highly depend upon their sizes, shapes and surrounding environments.[6–8] At the atomic scale, none of single NPs has identical sizes, shapes and surface morphologies. Therefore, none of single NPs has the identical LSPR spectrum. Such unique optical properties enable individual NPs to be distinguished and identified by MSIS. Thus, each NP can serve as a distinguished optical probe. These intrinsic plasmonic optical properties of single NPs enable PHOTON to effectively avoid the need of repeatedly photobleaching and reactivating of fluorescence molecules, which promises that PHOTON

Department of Chemistry and Biochemistry, Old Dominion University, Norfolk, VA, 23529, USA. E-mail: xhxu@odu.edu; Web: www.odu.edu/sci/xu/xu.htm; Fax: +1 757 683-5698; Tel: +1 757 683-5698

† Electronic supplementary information (ESI) available. See DOI: 10.1039/c1nr10182j

This journal is © The Royal Society of Chemistry 2011

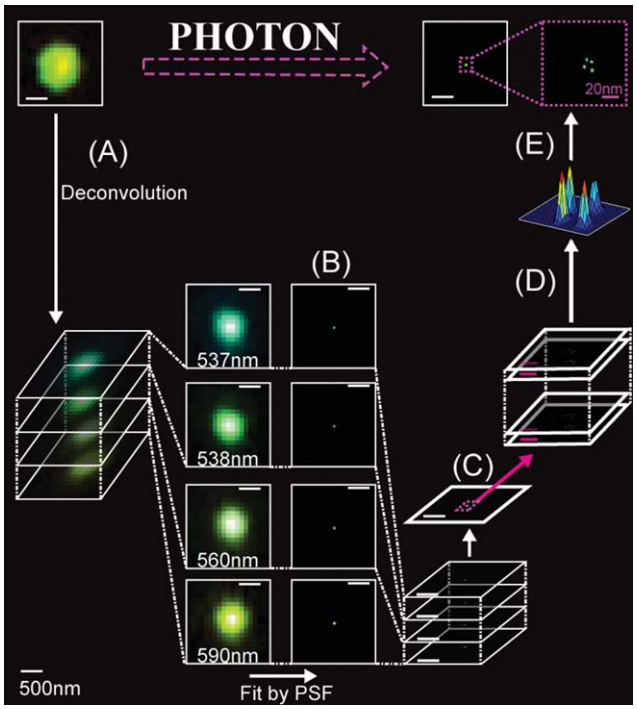


Fig. 1 Illustration of design of PHOTON for mapping individual ligands (biotin) and their binding sites with single protein molecules (streptavidin) in single protein–ligand complexes: (A) deconvolution of LSPR spectrum of single SMNOBS (AgMMUA–biotin) bound with single streptavidin molecules (AgMMUA–biotin–streptavidin NPs) using LSPR spectrum of individual SMNOBS *via* Cauchy–Lorentz distribution model (see ESI†). (B) Determination of centroids of individual SMNOBS bound with single streptavidin molecules using PSF. (C) Multiple (20) measurements of (A–B). (D) Locating precise positions of individual SMNOBS bound with streptavidin in single complexes using 2D Gaussian fitting. (E) Assembly of (D) into super-resolution images of individual SMNOBS in the complex at 1.2 nm resolution.

has much higher temporal resolution and superior photostability and advantages over fluorescence-based nanoscopes.

To demonstrate a proof-of-concept, we utilized PHOTON to image single biotin molecules bound with individual streptavidin molecules and their binding sites in single biotin–streptavidin complexes. Each streptavidin molecule has four biotin binding sites and the distance between two neighboring binding sites is 2.98 nm. Thus, each streptavidin molecule can bind either with one, two, three, or four biotin molecules,[9] which serves as an excellent model for mapping the binding sites of single protein–ligand complexes. Notably, protein–ligand interactions and binding complexes play a wide variety of roles in cellular functions. Thus, probing of protein–ligand complexes and locating of their binding sites in their native environments in real time can lead to better understanding of their roles in cellular functions.

Ag NPs with average diameters of 2.6 ± 1.1 nm (1.5–3.7 nm) were synthesized and characterized, as we described previously.[10,11] LSPR spectra of single Ag NPs show peak-wavelengths (λ_{max}) ranging from 450 to 511 nm and FWHM from 56 to 66 nm (Fig. S1 in the ESI†). Ag NPs were then functionalized with a mixed monolayer of MUA (11-mercaptoundecanoic acid) and MCH (6-mercapto-1-hexanol) using interaction of their thiol groups (–SH) with the surface of Ag NPs to prepare AgMMUA NPs. AgMMUA NPs with one MUA per NP were prepared by controlling the molar ratios of functional groups (mixed monolayer of MUA and MCH) on the surface of single Ag NPs (Fig. 2A), as characterized by NMR spectra (Fig. S2†) and close-packing model.[10] Single biotin molecules were attached onto single AgMMUA NPs (one biotin per NP) by covalently conjugating the amine group of AHH–biotin to one carboxyl group of MUA (one per NP) *via* a peptide bond, creating intrinsic single molecule nanoparticle optical biosensors (SMNOBS, AgMMUA–biotin NPs) with one biotin per NP (Fig. 2A and B).[10] Since there is only one carboxyl group (MUA) per NPs, only one biotin molecule can be attached onto one NP, generating SMNOBS. Each NP (SMNOBS) has one biotin molecule. Thus, SMNOBS can be used to track the binding of single biotin molecules with individual streptavidin molecules and to map their individual binding sites in single streptavidin–biotin complexes.

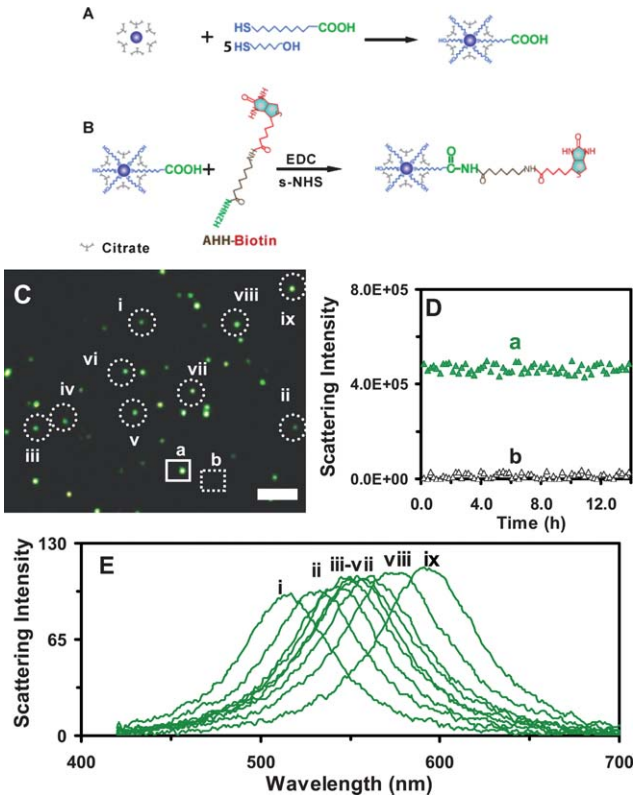


Fig. 2 Synthesis and characterization of individual SMNOBS (AgMMUA–biotin NPs). (A) Functionalization of Ag NPs with the mixed monolayer of MUA and MCH using interaction of their thiol groups (–SH) with the surface of Ag NPs to prepare AgMMUA. (B) Synthesis of SMNOBS by linking carboxyl group of the MUA (one per NP) with the amine group of biotin–AHH *via* a peptide bond mediated by EDC and sulfo-NHS. (C) Dark-field optical images, (D) photostability, and (E) LSPR spectra of individual SMNOBS show single plasmonic green NPs with λ_{max} from 518 to 592 nm and its FWHM from 65 to 72 nm, and SMNOBS resist photodecomposition and blinking. The LSPR spectra of single SMNOBS circled in (C) and labeled as (i–ix) are shown in (E). The plots of scattering intensity of representative one SMNOBS squared and labeled as (a) with background in (b) *versus* time are shown in (D). The 100 of individual SMNOBS were characterized. Scale bar in (C) is 5 μm, showing distances among individual SMNOBS, but not their sizes, due to the optical diffraction limit.

This journal is © The Royal Society of Chemistry 2011

Optical images, scattering intensity and LSPR spectra of individual SMNOBS (Fig. 2C–E), show distinct λ_{max} from 518 to 590 nm, attributing to high dependence of their LSPR spectra on their sizes, shapes and surrounding environments.[6–8] Notably, LSPR spectra of individual SMNOBS in individual pixels (length of each square pixel = 100 nm) were distinguished and isolated rapidly and simultaneously by MSIS with a wavelength accuracy of 1 nm. Furthermore, scattering intensity of single SMNOBS remains constant under continuous irradiation of dark-field illumination for 14 h (Fig. 2D), showing superior photostability (non-photobleaching, non-blinking) over fluorescence molecular probes.

Binding affinity of SMNOBS with streptavidin was measured using the approaches as described in the ESI†.[10,12] The result in Fig. S3† shows that their binding affinity (3.2×10^{15}) agrees well with those reported in the literature,[9,13,14] suggesting that the biotin molecules conjugated with AgMMUA NPs maintain their affinity and NPs do not create steric effects on their binding with streptavidin.

Far-field optical images of individual SMNOBS bound with streptavidin (AgMMUA–biotin–streptavidin NPs) in Fig. 3A show that multiple individual AgMMUA–biotin–streptavidin NPs were acquired simultaneously using dark-field optical microscopy and spectroscopy (DFOMS). Single AgMMUA–biotin–streptavidin NPs look much larger than their actual sizes (Fig. 3B), due to the optical diffraction limit.

The broad LSPR spectrum of single AgMMUA–biotin–streptavidin NPs shows a λ_{max} (FWHM) of 543 (84) nm (Fig. 3C-i), which was deconvoluted using LSPR spectra of individual SMNOBS (Fig. 2E) *via* the Cauchy–Lorentz distribution model (see ESI†), generating four spectra with λ_{max} (FWHM) at (a) 537 (63), (b) 538 (63), (c) 560 (62), and (d) 590 (65) nm (Fig. 3C, a–d). Thus, the green spot in Fig. 3B contains four SMNOBS bound with one streptavidin molecule. The image of each bound SMNOBS with its deconvoluted spectrum in (a–d) was fitted by PSF to determine its precise location (centroids) (Fig. 3D). The sum of LSPR spectrum of four individual SMNOBS at its individual centroid (Fig. 3C-ii) shows a λ_{max} (FWHM) of 543 (85) nm, which agrees well with the un-deconvoluted spectrum in Fig. 3C-i. The result validates the successful deconvolution of the LSPR spectrum in Fig. 3C-i.

The measurements and data analysis described in Fig. 3 were repeated 20 times, generating the distribution of centroids of each bound SMNOBS (Fig. 4A), which was fitted by 2D Gaussian to determine its location with statistic accuracy (Fig. 4B and C), as described in the ESI†. LSPR spectrum of each bound SMNOBS at its location (Fig. 4D) shows λ_{max} (FWHM) of (a) 537 (67), (b) 538 (67), (c) 560 (66), and (d) 590 (64) nm, which agrees excellently with the spectrum in Fig. 3C (a–d), respectively. This result further demonstrates the successful deconvolution of LSPR spectrum of AgMMUA–biotin–streptavidin NPs.

Using the same approach, LSPR spectrum of AgMMUA–biotin–streptavidin NPs (circled in Fig. 3A) was deconvoluted, the centroids of individual SMNOBS bound with streptavidin in each complex were determined using PSF. The distributions of their centroids were fitted by 2D Gaussian (Fig. S4–S7†). The contour plots of the 2D-Gaussion fitting of the distributions of centroids of individual SMNOBS bound with streptavidin show three or two biotin molecules (SMNOBS) in each binding complex with their precise locations (Fig. 4E and F).

A minimum of 100 AgMMUA–biotin–streptavidin NPs with either four, three, two, or one SMNOBS bound with each

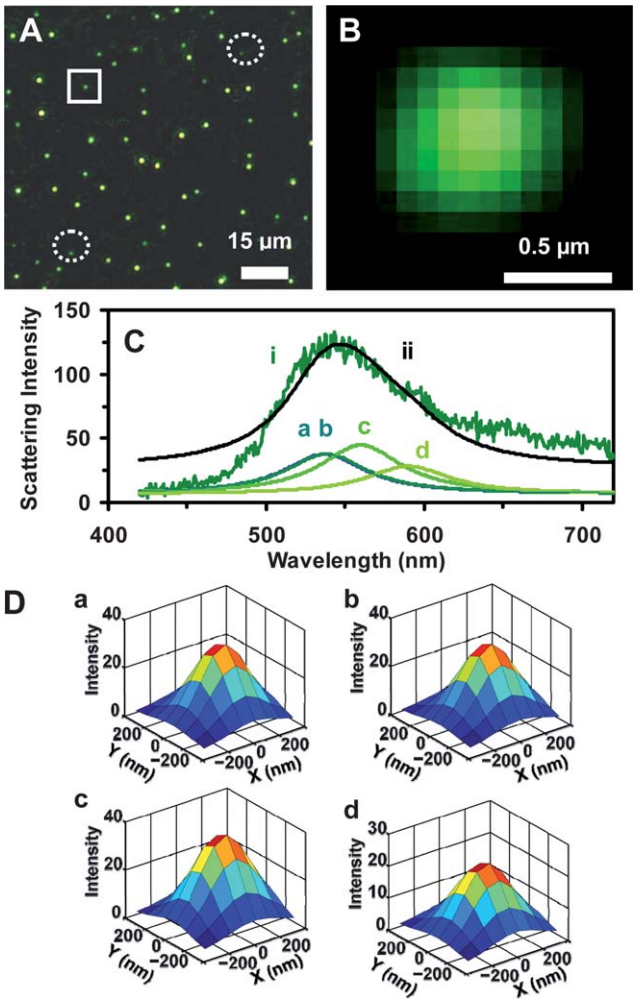


Fig. 3 Mapping of centroids (precise locations) of four individual SMNOBS bound with single streptavidin molecules using deconvolution and PSF. (A) Dark-field optical images of single AgMMUA–biotin–streptavidin NPs. (B) Zoom-in image of the NPs squared in (A). (C): (i) LSPR spectrum of the NPs in (B); (a–d) deconvoluted LSPR spectrum of individual SMNOBS bound with streptavidin; and (ii) sum of deconvoluted LSPR spectra of (a–d) show λ_{max} (FWHM) at: (i) 543 (84); (ii) 543 (85); (a) 537 (63); (b) 538 (63); (c) 560 (62); (d) 590 (65) nm. (D) Plots of scattering intensity of individual SMNOBS bound with streptavidin, with deconvoluted LSPR spectrum of (a–d) in (C), *versus* their locations, respectively. As determined by PSF, the precise locations of individual SMNOBS bound with a streptavidin molecule in (a–d) are (50.8, 44.6), (58.6, 48.4), (58.2, 56.6), and (49.2, 52.8) nm, respectively, according to their locations in the image.

streptavidin were studied, and the precise locations (centroids) of individual SMNOBS were determined (Fig. 3 and 4 and Fig. S4–S7†). Using these precise locations, we calculated the average distances between two neighboring SMNOBS in each complex as 8.8 ± 0.3, 8.6 ± 0.9, and 8.5 ± 1.1 nm, respectively.

HRTEM images of the AgMMUA–biotin–streptavidin NPs (Fig. 5A) show clusters of two, three or four NPs with average distances between two neighboring NPs at 8.7 ± 1.7. 8.7 ± 1.3 and 9.0 ± 1.7, respectively, which agree well with those measured using the precise locations (centroids) of individual SMNOBS imaged by PHOTON (Fig. 4). The distributions (%) of the complexes

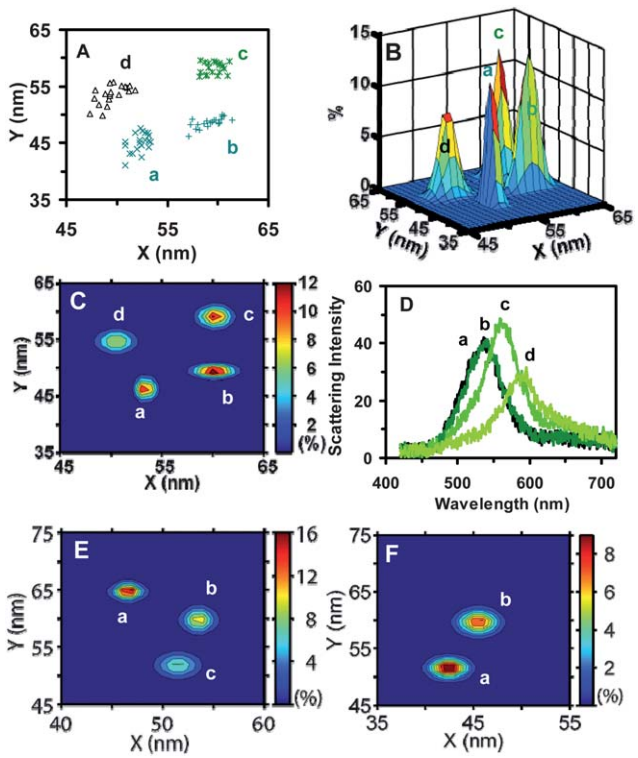


Fig. 4 Nanometre-resolution imaging of individual SMNOBS bound with single streptavidin molecules in single biotin–streptavidin complexes using PHOTON. (A) Plots of distributions of precise locations of single SMNOBS bound with a streptavidin molecule determined by PSF (Fig. 3D). Twenty points are 20 repeated measurements of precise locations of each SMNOBS, as those described in Fig. 3. (B) 2D Gaussian fitting of the distributions (probabilities, %) of 20 precise locations of each NP in (A). (C) The contour plots of (B) show precise locations of single NPs in (a–d): (53.5 ± 1.3, 46.2 ± 1.3), (60.2 ± 2.5, 49.4 ± 0.8), (60.2 ± 2.0, 59.0 ± 1.3), and (50.5 ± 2.0, 54.6 ± 1.3) nm. (D) LSPR spectrum of single SMNOBS at the locations in (C) shows λ_{max} (FWHM): (a) 537 (67), (b) 538 (67), (c) 560 (66), and (d) 590 (64) nm. (E and F) Using the same approaches, two representative AgMMUA–biotin–streptavidin NPs circled in Fig. 3A were analyzed (see Fig. S4–S7†). Their contour plots of (E) and (F) show three or two SMNOBS bound with a streptavidin molecule with locations at: (E) (46.0 ± 0.7, 64.0 ± 0.9); (52.1 ± 0.8, 59.2 ± 1.2); and (51.2 ± 1.1, 51.2 ± 1.2) nm; and (F) (41.9 ± 1.1, 51.3 ± 1.2) and (45.0 ± 1.3, 59.2 ± 1.2) nm, respectively. Distances among two neighboring NPs calculated from these locations are 8.6 ± 0.9 and 8.5 ± 1.1 nm, respectively. A minimum of 100 complexes, each bound either to one, two, three, or four biotin molecules, are analyzed using both PHOTON and HRTEM (Fig. 5).

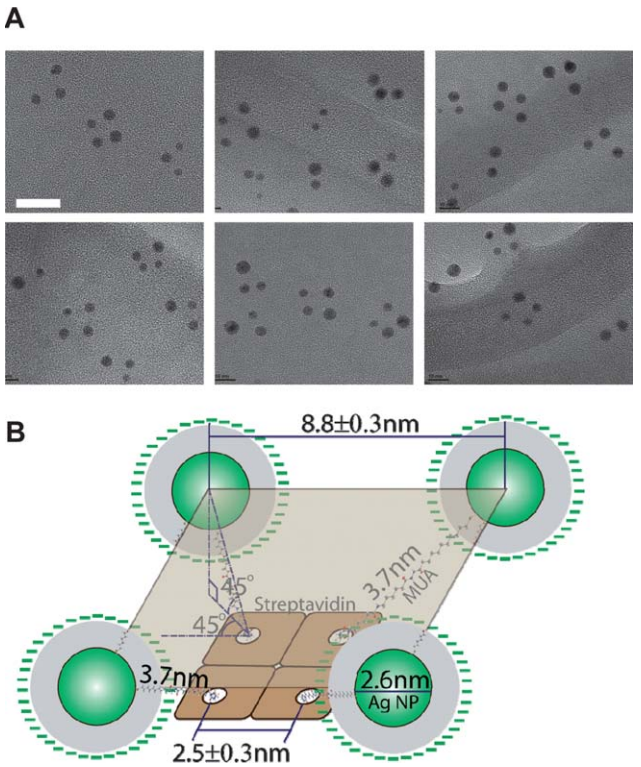


Fig. 5 Mapping of single biotin molecules and their binding sites in single streptavidin molecules using HRTEM and PHOTON. (A) HRTEM images of single SMNOBS bound with streptavidin show the clusters of two, three and four NPs with distances among two neighboring NPs at 8.7 ± 1.7, 8.7 ± 1.3, and 9.0 ± 1.7 nm, respectively. (B) The proposed structure of the AgMMUA–biotin–streptavidin complex with distances between two neighboring biotin binding sites calculated from their precise locations at 2.5 ± 0.3 nm, determined by PHOTON. Scale bar in (A) is 20 nm.

(AgMMUA–biotin–streptavidin NPs), each with one, two, three, or four SMNOBS (biotin) determined by PHOTON and HRTEM, are in an excellent agreement. There are 9%, 29%, 35%, and 27% of the complexes with one, two, three, or four biotin molecules (SMNOBS), respectively, which are calculated by dividing the number of complexes with one, two, three, or four SMNOBS with the total number of the complexes.

Notably, molar ratios of SMNOBS to streptavidin at 1 to 10 were used to prepare the samples, purposely creating a mixture of one to four biotin molecules per streptavidin molecule to determine whether PHOTON could effectively resolve single SMNOBS in each complex.

The surface of SMNOBS is negatively charged with ζ potential of −(7.4 ± 0.8) mV, which prevents their aggregation in solution. Therefore, four SMNOBS bound with a streptavidin molecule repel each other, situating in the longest distance between each other with the long linker (MUA), which connects Ag NPs with bound biotin at 45°, as illustrated in Fig. 5B. MUA serves as a linker to conjugate amine groups of the molecules (*e.g.*, ligand, protein) with carboxyl group of MUA on the NPs *via* peptide bonds. Notably, the long linker (MUA) avoids any possible steric effects of NPs on the binding affinity and function of biotin.

The average distances between two neighboring SMNOBS in each complex determined using the precise location of each SMNOBS imaged by PHOTON are 8.8 ± 0.3 nm. The length of MUA–AHH–biotin and average radius of single Ag NPs are 3.7 and 1.3 nm, respectively. Therefore, average distances between two neighboring biotin binding sites in a streptavidin molecule are 2.5 ± 0.3 nm, which agrees well with those (2.98 nm) determined using crystallography (PDB 1D: 1SWE).[9] Notably, the binding complexes were imaged in solution by PHOTON. Thus, the linker (MUA) between Ag NPs and biotin bound with streptavidin may allow the motion of individual NPs, leading to various distances between two neighboring NPs (Fig. 4 and 5). Remarkably, PHOTON unambiguously distinguishes them, demonstrating its incredible suitability for mapping the binding sites of the protein–ligand complexes.

This journal is © The Royal Society of Chemistry 2011

To determine the spatial resolution of PHOTON, the number of photons (N) that each bound SMNOBS scattered and recorded by a CCD camera was measured by subtracting the average background intensity from integrated intensity of each SMNOBS in each area with 20×20 pixels, as we described previously.[10,15] Notably, Ag NPs scatter all visible wavelengths of light as they are illuminated by a microscope white-light illuminator. Thus, scattering intensity of single SMNOBS is the sum of scattering intensity at each given wavelength of its LSPR spectrum. One electron count of a CCD camera with a 12-bit scale is equal to the collection of about 3.5 electrons. Thus, the number of photons that single SMNOBS bound with streptavidin scatters, ranging from 7.8×10^3 to 1.2×10^4 with an average of $(9.3 \pm 0.1) \times 10^3$. With a standard deviation (S) of PSF of (149.8 ± 17.1) nm (Fig. 3D), a standard deviation of background noise (b) of (3.4 ± 0.2), and each length of square pixel size of a CCD camera (a) of 100 nm, PHOTON has achieved 1.2 nm spatial resolution with averages of (1.6 ± 0.2) nm, as calculated by eqn (1).

Notably, quantum efficiency (QE) of CCD camera at a given wavelength from 420 to 720 nm ranges from 0.43 to 0.63. Thus, individual SMNOBS scatters more photons than those collected by a CCD. With a more sensitive CCD camera (QE $\geq$ 0.8), PHOTON with tiny NPs (2.6 ± 1.1 nm) as imaging probes would have achieved Ångstrom spatial resolution. Furthermore, scattering intensity of single Ag NPs is proportional to their volume.[6,7] As their sizes increase, the number of photons that single NPs scatter increases. Thus, PHOTON with slightly larger NPs (diameter $\geq$ 4) as imaging probes would potentially achieve Ångstrom spatial resolution. Therefore, current spatial resolution (1.2 nm) of PHOTON is limited technologically, but not fundamentally.

The temporal resolution of PHOTON depends upon exposure time at each given wavelength to gain sufficient S/N ratios of single SMNOBS. The observational resolution depends upon the spectral resolution, wavelength range and exposure time. For 1 nm spectral resolution with 300 nm wavelength range (420–720 nm) and 100 ms exposure time at each given wavelength, it takes 30 s to obtain 1 447 680 spectra of every single pixel of a full-frame image (1392×1040). Therefore, the temporal and observational resolutions are 100 ms and 30 s, respectively. Notably, single SMNOBS has been detected with 5 ms exposure time using MSIS.[10,11] The wavelength ranges of single SMNOBS could be narrowed down to $\lambda_{max} \pm 5$ nm (10 nm within λ_{max} of LSPR spectra of single NPs), which can potentially achieve 5 ms temporal and 50 ms observational resolution.

With the intrinsic polydisperse LSPR spectra of individual SMNOBS, PHOTON has imaged numerous individual molecules (SMNOBS) at nm resolution simultaneously, overcoming the need of switching on and off fluorophores. Unlike fluorescence probes that required the single-wavelength excitation sources (*e.g.*, laser), SMNOBS are irradiated by a standard microscopic white-light illuminator (halogen lamp), which effectively avoids auto-fluorescence of proteins, reduces the background noise and increases detection sensitivity.[10,12] Unlike single fluorophores and QDs, SMNOBS show superior photostability (non-photobleaching, non-blinking, Fig. 2D). Notably, we have demonstrated that single Ag NPs can serve as photostable nanophotonic probes for sensing and imaging of single molecules and dynamic events of interest in single living cells and embryos for any desired period of time.[10,12,15–17]

Furthermore, Ag NPs offer the highest quantum yield (QY) of Rayleigh scattering and their scattering intensity is proportional to their volumes.[6,7] For Ag NPs with a diameter of 2.6 ± 1.1 nm, scattering intensity of single NPs is about 10^4 times higher than that of a fluorophore molecule (*e.g.*, R6G), suggesting that PHOTON can achieve higher sensitivity and higher spatial resolution than fluorescence microcopy, as described by eqn (1).

The ultrasmall NPs avoid steric effects, offer high spatial resolution, and provide larger surface area-to-volume ratios for higher sensing sensitivity of SMNOBS.[10,12] They also offer small detection volume, which reduces noise and thereby increases sensitivity for single molecule detection (SMD).[10,12,18] Notably, sizes of our NPs (2.6 ± 1.1 nm) are smaller than GFP (length 4.7 nm and diameter of 3.4 nm) (PDB codes: 3ogo and 1EMA).[19–21] Any ligands or proteins of interest can be directly conjugated with AgMMUA NPs to prepare SMNOBS, which avoids the need of using antibody (maximum length 15.3 nm) (PDB code: 1IGT) or anti-antibody sandwich assays.[19–21] Taken together, these unique properties of SMNOBS enable them to serve as photostable multicolor optical probes for imaging of single molecules with superior spatial and temporal resolution.

In summary, we have successfully developed PHOTON, which used SMNOBS as photostable plasmonic optical probes, for imaging of individual ligand (biotin) molecules and their binding sites in single protein–ligand (streptavidin–biotin) complexes at 1.2 nm spatial resolution and 100 ms temporal (30 s observation) resolution using far-field optical microscopy. SMNOBS serves as nanoprobes for both PHOTON and HRTEM, which enables locating individual NPs using both PHOTON and HRTEM. Thus, it enables the validation of PHOTON for achieving nanometer imaging spatial resolution. Notably, PHOTON could potentially achieve 5 ms temporal resolution (50 ms observation resolution) and Ångstrom spatial resolution. PHOTON represents major breakthrough in sub-diffraction optical imaging with distinguished advantages, including superior photostability, superior spatial and temporal resolution, and no need of laser excitation sources. Thereby, it effectively avoids auto-fluorescence of proteins and phototoxicity for imaging living organisms. PHOTON offers the feasibility of mapping binding sites of proteins and imaging of living organisms at Ångstrom resolution in real time.

Acknowledgements

This work is supported in part by NSF (NIRT: CBET 0507036) and NIH (R01 GM076440; 3R01GM076440-04S1; 3 R01 GM076440-01S1).

References

1 E. B. Abbe, *Arch. Mikrosk. Anat.*, 1873, **9**, 413–468.
2 R. E. Thompson, D. R. Larson and W. W. Webb, *Biophys. J.*, 2002, **82**, 2775–2783.
3 W. Lukosz, *J. Opt. Soc. Am.*, 1966, **56**, 1463–1472.
4 J. Lippincott-Schwartz and S. Manley, *Nat. Methods*, 2009, **6**, 21–23.
5 R. Y. Tsien and A. Waggoner, in *Handbook of Biological Confocal Microscopy*, ed. J. B. Pawley, Plenum, New York, 2nd edn, 1995, pp. 267–280.
6 U. Kreibig and M. Vollmer, *Optical Properties of Metal Clusters*, Springer, Berlin, 1995, pp. 14–123.
7 G. Mie, *Ann. Phys.*, 1908, **25**, 377–445.
8 T. Huang and X.-H. N. Xu, *J. Mater. Chem.*, 2010, **20**, 9867–9876.
9 W. A. Hendrickson, A. Pähler, J. L. Smith, Y. Satow, E. A. Merritt and R. P. Phizackerley, *Proc. Natl. Acad. Sci. U. S. A.*, 1989, **86**, 2190–2194.
10 T. Huang, P. D. Nallathamby and X.-H. N. Xu, *J. Am. Chem. Soc.*, 2008, **130**, 17095–17105.

11 P. D. Nallathamby, T. Huang and X.-H. N. Xu, *Nanoscale*, 2010, **2**, 1715–1722.
12 T. Huang, P. D. Nallathamby, D. Gillet and X.-H. N. Xu, *Anal. Chem.*, 2007, **79**, 7708–7718.
13 M. Gonzalez, L. A. Bagatolli, I. Echabe, J. L. R. Arrondo, C. E. Argarana, C. R. Cantor and G. D. Fidelio, *J. Biol. Chem.*, 1997, **272**, 11288–11294.
14 O. H. Laitinen, V. P. Hytönen, H. R. Nordlund and M. S. Kulomaa, *Cell. Mol. Life Sci.*, 2006, **63**, 2992–3017.
15 P. D. Nallathamby, K. J. Lee and X.-H. N. Xu, *ACS Nano*, 2008, **2**, 1371–1380.
16 X.-H. N. Xu, J. Chen, R. B. Jeffers and S. V. Kyriacou, *Nano Lett.*, 2002, **2**, 175–182.
17 P. D. Nallathamby, K. J. Lee, T. Desai and X.-H. N. Xu, *Biochemistry*, 2010, **49**, 5942–5953.
18 X. H. Xu and E. S. Yeung, *Science*, 1997, **275**, 1106–1109.
19 L. J. Harris, S. B. Larson, K. W. Hasel and A. McPherson, *Biochemistry*, 1997, **36**, 1581–1597.
20 M. H. Kubala, O. Kovtun, K. Alexandrov and B. M. Collins, *Protein Sci.*, 2010, **19**, 2389–2401.
21 M. Ormo, A. B. Cubitt, K. Kallio, L. A. Gross, R. Y. Tsien and S. J. Remington, *Science*, 1996, **273**, 1392–1395.

 This journal is © The Royal Society of Chemistry 2011

Electronic Supplementary Material (ESI) for Nanoscale
This journal is © The Royal Society of Chemistry 2011

On-Line Supplementary Information

Multicolored Nanometer-Resolution Mapping of Single Protein-Ligand Binding Complexes Using Far-Field Photostable Optical Nanoscopy (PHOTON)

Tao Huang and Xiao-Hong Nancy Xu*

Department of Chemistry and Biochemistry, Old Dominion University, Norfolk, VA 23529

The on-line supplementary information includes:

(A) Materials and Methods

(B) Seven Supplementary Figures and Figure Caption

Fig. S1: Characterization of sizes and plasmonic optical properties of single Ag NPs

Fig. S2: NMR characterization of functional groups attached on the surface of Ag NPs.

Fig. S3: Characterization of binding activities of SMNOBS (AgMMUA-Biotin NPs)

Fig. S4: Mapping of centroids of three SMNOBS bound with single streptavidin molecules in biotin-streptavidin complexes using deconvolution and point spread function (PSF).

Fig. S5: Nanometer-Resolution imaging of three SMNOBS bound with single streptavidin molecules in single biotin-streptavidin complexes using PHOTON.

Fig. S6: Mapping of centroids of two SMNOBS bound with single streptavidin molecules in single biotin-streptavidin complexes using deconvolution and PSF.

Fig. S7: Nanometer-Resolution imaging of two SMNOBS bound with single streptavidin molecules in single biotin-streptavidin complexes using PHOTON.

* To whom correspondence should be addressed: Email: xhxu@odu.edu; www.odu.edu/sci/xu/xu.htm; Tel/fax: (757) 683-5698

Electronic Supplementary Material (ESI) for Nanoscale
This journal is © The Royal Society of Chemistry 2011

A. Materials and Methods

Reagents and Supplies

Sodium borohydride (≥ 98%), sodium citrate dihydrate (≥ 99%), silver nitrate (≥ 99.9%), hydrogen peroxide (30%), polyvinylpyrrolidone (PVP), 11-mercaptoundecanoic acid (MUA ≥ 95%), 6-mercapto-1-hexanol (MCH) (≥ 97%), (+)-biotinamidohexanoic acid hydrazide (biotin-AHH) (95%), and streptavidin were purchased from Sigma-Aldrich. *N*-hydroxysulfosuccinimide (Sulfo-NHS ≥ 98.5%) and 1-Ethyl-3-[3-dimethylaminopropyl]-carbodiimide hydrochloride (EDC ≥ 99%) were purchased from Pierce. Nanopure deionized water (DI, 18 MΩ, Barnstead) was used to rinse glassware for synthesis of Ag nanoparticles (NPs) and to prepare all solutions, including 10 mM phosphate buffer saline (PBS) (pH = 7.4, 10 mM of phosphate buffer and NaCl).

Synthesis and Characterization of SMNOBS (AgMMUA-Biotin)

2.6 ± 1.1 nm Ag NPs

We synthesized and characterized Ag NPs with average diameters of 2.6 ± 1.1 nm and functionalized Ag NPs with a mixed monolayer of MUA and MCH, as we described previously.[1-2] Briefly, $AgNO_3$ (0.11 mM), sodium citrate (1.91 mM), PVP (0.052 mM), and H_2O_2 (25.0 mM) in nanopure DI water (42.3 mL) were prepared freshly and well mixed under stirring. $NaBH_4$ (150 μL, 100 mM) was added into the mixture, which was stirred for another 3 h to synthesize Ag NPs. The solution was filtered using 0.2 μm membrane filters, and immediately used for characterization and for preparation of AgMMUA NPs. TEM samples of Ag NPs were characterized using high-resolution transmission electron microscopy (HRTEM) (JEOL JEM-2100F), showing diameters of Ag NPs at 2.6 ± 1.1 nm (Fig. S1). The Ag NP solution was also immediately characterized using our dark-field optical microscopy and

Electronic Supplementary Material (ESI) for Nanoscale
This journal is © The Royal Society of Chemistry 2011

spectroscopy (DFOMS, also named as SNOMS by us), UV-vis spectroscopy (Hitachi U3310), and dynamic light scattering (DLS) (Nicomp 380ZLS particle sizing system). Concentration of Ag NPs was calculated as 154 nM, using the same approaches as we reported previously. [3-7]

We have fully described the design and construction of our DFOMS for real-time imaging and spectroscopic characterization of single NPs in solutions,[3, 8-10] in single living cells, [1, 7, 11-16] and in single zebrafish embryos.[3, 8-9] In this study, dark-field optical microscope is equipped with a dark-field condenser (Oil 1.43-1.20, Nikon), a microscope illuminator (Halogen lamp, 100 W), and a 100x objective (Nikon Plan fluor 100x oil, SL. N.A. 0.5-1.3, W.D. 0.20 mm). The microscope is coupled with Nuance Multispectral Imaging System (N-MSI-VIS-FLEX, CRI), CCD camera equipped with liquid-crystal tunable filter (LCTF).[17]

AgMMUA NPs

AgMMUA NPs were prepared by mixing MUA (10 mM) and MCH (90 mM) in ethanol with freshly prepared Ag NPs (50 mL, 154 nM) to have final concentrations of MUA, MCH and Ag NPs at 0.1 mM, 0.9 mM, and 152 nM, respectively.[1, 11] The solutions were then stirred for 24 h to attach MUA and MCH onto the surface of NPs via the interaction of –SH groups with NPs and SN2 replacement reaction of citrate molecules with MUA and MCH (Fig. 2A in main text). The AgMMUA NPs were washed twice using nanopure DI water to remove excess MUA and MCH using centrifugation (Beckman Optima L90k, 50 Ti rotor, 30,000 rpm at 4°C for 60 min), and immediately characterized using DFOMS, UV-vis spectroscopy, and DLS.

Notably, the attached functional groups (MUA and MCH) on the surface of NPs changed the dielectric constant of NP, which led to the red shift of LSPR spectra of Ag NPs, from blue color to green colors, as shown in Figures S1-D and 2E. The yields of preparation of AgMMUA NPs from Ag NPs were characterized using DFOMS at single NP resolution and

Electronic Supplementary Material (ESI) for Nanoscale
This journal is © The Royal Society of Chemistry 2011

using UV-vis spectroscopy for bulk NP solution. The results show the average yield of 92.0 ± 0.8, which confirms the superior strong interaction of –SH group of MUA and MCH with the surface of Ag NPs.

NMR samples of AgMMUA were immediately prepared by drying the washed AgMMUA NPs using lyophilizer (VirTis) and dissolving AgMMUA NPs (50 mg) in D_2O (1 mL), and further characterized using NMR (400 MHz, Bruker). NMR spectra in Fig. 2S show molar ratio of citrate : MCH : MUA : PVP = 33 : 5 :1 :0.03. One MUA per NPs was determined by a close-packing model, as we described previously. [1]

AgMMUA-Biotin NPs (SMNOBS)

We used a two-step method to conjugate the carboxyl group of AgMMUA with amine group of biotin-AHH via a peptide bond using EDC and sulfo-NHS as mediators (Fig. 2B in the text). EDC (77 μmol) and sulfo-NHS (7.7 μmol) were added to AgMMUA aqueous solution (50 mL, 154 nM), forming AgMMUA-s-NHS esters. After stirring at room temperature for 40 min, the AgMMUA-s-NHS was isolated using a Centriprep YM-30 (Millipore) by centrifugation at 1500 rcf (relative-centrifuge-force) for 5 min to remove excess EDC and sulfo-NHS, and then re-dissolved in the PBS buffer.

In the second step, biotin-AHH was added to AgMMUA-s-NHS in the buffer at a molar ratio of biotin to AgMMUA of 0.97. The solution was mixed using a rotary shaker at room temperature for 2 h and then at 4 ºC for 12 h. The AgMMUA-Biotin NPs were washed using the PBS buffer (10 mM) to remove excess biotin-AHH using centrifugation. The pellet was resuspended in the buffer, which was characterized using DFOMS, UV-vis spectroscopy, and DLS. Each AgMMUA NP could only conjugate with one biotin molecule to create SMNOBS,

Electronic Supplementary Material (ESI) for Nanoscale
This journal is © The Royal Society of Chemistry 2011

because only one carboxyl group is available per AgMMUA NP, as characterized by NMR spectra (Fig. S2) and a close-packing model, as we described previously.[1] Thus, one AgMMUA-biotin NP (SMNOBS) has only one biotin molecule, which can be used to track its binding with a single streptavidin molecule and to map its individual binding sites in individual protein-ligand (streptavidin-biotin) complexes.

AgMMUA-Biotin-Streptavidin NPs

To determine the possible steric effects of NPs on the binding affinity of biotin with streptavidin, we measured the binding constant (affinity) of AgMMUA-Biotin NPs with streptavidin in the PBS buffer by measuring the absorbance of AgMMUA-Biotin NPs (60 nM) incubated with streptavidin (600 nM) over time.[1, 11] The UV-vis absorption spectra were measured at room temperature every 5 min for the first 2 h and at every 2.5-25 h after that until 48 h. The mixture was stored at 4 ºC between each spectroscopy measurement.

UV-vis absorption spectra of AgMMUA-Biotin NPs show stable peak wavelengths at 403 ± 1 nm (Fig. S3A) with the extinction coefficient (molar absorptivity, ε) of 9.5×10^6 $M^{-1}cm^{-1}$, which was determined by the Beer-Lambert Law with a dilution series of AgMMUA-Biotin NPs solutions. As AgMMUA-Biotin NPs were incubated with Streptavidin, absorbance of the spectra decreased over incubation time with its peak wavelength (403 nm) and FWHM remaining essentially unchanged (Fig. S3A), suggesting that AgMMUA-Biotin-Streptavidin NPs did not contribute significantly to the absorption. Such interesting phenomena might be attributable to the decrease of reflectivity of NPs due to the surface functional molecules, leading to the decrease of scattering and absorption intensity.[1, 11]

The results further confirm one biotin molecule per NP and the successful preparation of SMNOBS. Otherwise, if there were multiple biotin molecules per NP, one NP can bind with

Electronic Supplementary Material (ESI) for Nanoscale
This journal is © The Royal Society of Chemistry 2011

more than one streptavidin molecule, which would lead to the aggregation of NPs and the red shift of UV-vis absorption spectrum.

A plot of the peak absorbance subtracted from baseline versus time in Fig. S3B exhibits high linearity during the first 30 min of the incubation time (Fig. S3C) and then remains constant, suggesting that the binding of SMNOBS with streptavidin is a first-order reaction, as those we calculated previously.[11] Binding constant (3.2×10^{15}) and associate rate constant ($6 \times 10^{2}\ M^{-1}s^{-1}$) are calculated using the approaches as we described previously,[1, 11] which agrees well with those reported in the literature.[18-20] The result in Fig. S3 demonstrates that the biotin conjugated with AgMMUA maintains its affinity and no steric effects of Ag NPs are observed.

Characterization of Photostability of SMNOBS

Photostability of single AgMMUA-Biotin NPs (SMNOBS) was characterized, using the same approach as we described previously.[1, 9] Sequential optical images of single SMNOBS were acquired using dark-field optical microscope equipped with MSIS, with exposure time of 100 ms and readout time of 40.6 ms, while these NPs were constantly irradiated under a dark-field microscope illuminator (100 W halogen) for 14 h.[1, 9] The illumination power at the sample stage (focal plane of dark field) was (0.070 ± 0.001) Watt during the experiment. Scattering intensity of individual NPs was measured over time to determine their photostability (Fig. 2D), showing that SMNOBS exhibits superior photostability (non-bleaching and non-blinking). More than 100 of SMNOBS were characterized to gain sufficient statistics to represent the bulk SMNOBS in solution at single NP resolution.

Electronic Supplementary Material (ESI) for Nanoscale
This journal is © The Royal Society of Chemistry 2011

Design and Data Analysis of PHOTON for Nanometer-Resolution Imaging of Single Biotin Molecules and their Binding Sites in Single Biotin-Streptavidin Complexes

Stacks of the plasmonic images (image cubes) of single AgMMUA-Biotin-Streptavidin NPs were acquired from 420 to 720 nm at each nm (1 nm spectral resolution) with 100 ms exposure time using Multispectral Imaging System (MSIS; CCD camera equipped with LCTF), as shown in Figs. 3A, S4A, S6A. The LSPR spectra of AgMMUA-Biotin-Streptavidin NPs were deconvoluted using individual LSPR spectrum of single SMNOBS via Cauchy-Lorentz distribution model (Figs. 3C, S4C, S6C), as described in Eq. [S1]. [21-24]

$$I(\lambda) = \sum_{i=1}^{n} \frac{a_i}{\left[1 + \left(\frac{\lambda - \lambda_i}{b_i}\right)^2\right]} \qquad [S1]$$

Where n is the total number of individual SMNOBS (AgMMUA-Biotin NPs), I(λ) is the scattering intensity of single NP clusters (AgMMUA-Biotin-Streptavidin NPs) at a given wavelength (λ), a_i is the peak intensity of the i^{th} NPs, λ_i is the peak wavelength (λ_{max}) of the i^{th} NPs, and b_i is the half of the FWHM of the LSPR spectrum of the i^{th} NPs.

Using Matlab curve fitting tools with the customized Eq. [S1], each spectrum of the NP clusters, as circled in Fig. 3A, was fitted. The range of a_i from 0 to infinity, the range of λ_i from 510 to 600 nm (based upon range of λ_{max} of LSPR spectra of all individual SMNOBS in Fig. 2E), and range of b_i from 25 to 45 (based upon FWHM of LSPR spectra of SMNOBS in Fig. 2E), were set for fitting the curves (spectra). The total number of single NPs in each cluster was determined by the best fitting curve of the spectrum. The fitting curves with different n values were compared and the best fitting curve with the highest regression (R^2) was selected.

Electronic Supplementary Material (ESI) for Nanoscale
This journal is © The Royal Society of Chemistry 2011

The LSPR spectrum of each NP (SMNOBS) can then be described by Eq. [S2]:

$$I_i(\lambda) = \frac{a_i}{\left[1 + (\frac{\lambda - \lambda_i}{b_i})^2\right]} \quad [S2]$$

Where $I_i(\lambda)$ is scattering intensity of the i^{th} NP at a given wavelength (λ). Notably, a_i, λ_i and b_i were determined by the spectral curve fitting using Eq. [S1], as described above.

Using the LSPR spectra of single SMNOBS (Figs. 3C: a-d; S2: a-c and S6: a-b) obtained from Eq. [S2], the image cubes of the NP clusters, as those shown in Fig. 3A, were unmixed (deconvoluted) at the given wavelength of each NP. For n number of NPs, n images were generated in TIFF format. Each image is the profile of scattering intensity of a single NP with the corresponding LSPR spectrum versus its location in the full frame of CCD array, as shown in Figs. 3D, S4D, and S6D.

The deconvolution (un-mixing) of each image cube was performed as described below using the software of MSIS, as each image cube of the NP clusters at each pixel is made up of a linear combination of LSPR spectra of individual NPs at the pixel. [25]

$$\mathbf{S}_{x,y} = L\mathbf{w} \quad [S3]$$

$$S_{x,y} = \begin{bmatrix} L_{11} & L_{12} & \dots & L_{1n} \\ L_{21} & L_{22} & \dots & L_{2n} \\ \dots & \dots & & \dots \\ L_{m1} & L_{m2} & \dots & L_{mn} \end{bmatrix} \begin{bmatrix} w_1 \\ w_2 \\ \dots \\ w_n \end{bmatrix} \quad [S4]$$

Where $\mathbf{S}_{x,y}$ is a vector containing multiple LSPR spectra at each pixel; L is a matrix with n LSPR spectra from n number of single NPs, m is the number of spectral channels, and **w** is vector of scattering intensity contributed by each NP in L matrix for each pixel in each image.

Electronic Supplementary Material (ESI) for Nanoscale
This journal is © The Royal Society of Chemistry 2011

Here L_{ji} is the scattering intensity, $I_i(j+419)$, of the i^{th} NP at the j^{th} channel (wavelength, $\lambda = j + 419$ nm, ranging from 420 to 720 nm, totally m of 301 channels). For example, L_{11}, L_{21}, … L_{m1} represents scattering intensity of the LSPR spectrum of the 1^{st} NP, and L_{1n} L_{2n} … L_{mn} represents scattering intensity of the LSPR spectrum of the n^{th} NP.

Note that w_i is the percent of scattering intensity of i^{th} NPs in total scattering intensity contributed by total number (n) of NPs in each pixel, as described in Eq. [S5].

$$I_{i,x,y}(\lambda) = w_i I_{x,y}(\lambda) \quad [S5]$$

Where $I_{i,x,y}(\lambda)$ is scattering intensity of the i^{th} NPs at a given wavelength (λ) in a pixel located in (x, y). $I_{x,y}(\lambda)$ is total scattering intensity of n NPs (undeconvoluted NP clusters) at the same given wavelength in the same pixel. Thus, sum of w_i ($w_1 + w_2 + \ldots + w_n$) is equal to one.

The least squares approximation was used to minimize the residuals (*e*) and to obtain the best values of **w,** as described below in Eq. [S6].

$$e = \left\| Lw - S_{x,y} \right\|^2 \quad [S6]$$

After deconvolution (unmixed) of each image cube, a grayscale image in TIFF format for each NP with a given LSPR spectrum was generated. The image of each NP was then fitted by PSF using 2D Gaussian distribution (Figs. 3D, S4D, S5D), as described in Eq. [S7].[26]

$$N_{x,y} = B + N_{00} e^{-\frac{1}{2}\left[\left(\frac{x-x_0}{S_x}\right)^2 + \left(\frac{y-y_0}{S_y}\right)^2 \right]} \quad [S7]$$

Electronic Supplementary Material (ESI) for Nanoscale
This journal is © The Royal Society of Chemistry 2011

Where (x_0, y_0) is centroid of a scattering point; $N_{x,y}$ is scattering intensity of a NP at the pixel (x, y); N_{00} is scattering intensity at the centroid (x_0, y_0); S_x and S_y are the widths of the PSF in x and y directions, respectively; and B is background intensity.

Center positions of the 2D-Gaussian fittings are the precise locations (centroids) of each NP. The standard deviations (SD) of the centroids were determined using FWHM of 2D-Gaussian fitting curves, as described in Eq. [S8]:

$$SD = \frac{FWHM}{2\sqrt{2\ln 2}} \approx \frac{FWHM}{2.355} \qquad [S8]$$

Using the same approaches, twenty image cubes (stack images of plasmonic images of NP clusters at each wavelength from 420-720 nm with 1-nm resolution) were taken and twenty precise locations for each NP were analyzed, as described above and shown in Figs. 4A, S5A and S7A. The 20 precise locations of each NP were then fitted by 2D-Gaussian distribution, as described in Eq. [S7] and as shown in Figs. 4B-C, S5B-C, and S7B-C. Peak position of the 2D Gaussian fitting curve for 20 precise locations of each NP was used to determine final precise location of each NP (SMNOBS) bound with single streptavidin molecules in single biotin-streptavidin complexes. Standard deviation of the precise location of each NP was determined using FWHM of the 2D Gaussian fitting curve, as described above in Eq. [S8].

Nanometer-Resolution Mapping of Individual Biotin Molecules and Their Binding Sites in Single Streptavidin-Biotin Complexes Using PHOTON

Streptavidin molecules were immobilized on microscopic slides by incubating the slides with streptavidin (0.25 mg/mL) for 60 min, and well rinsing the slides with the PBS buffer. The

Electronic Supplementary Material (ESI) for Nanoscale
This journal is © The Royal Society of Chemistry 2011

slides coated with streptavidin were incubated with SMNOBS (5.3 nM) in the buffer for 1 h and well rinsed with the buffer. A microchamber was created by sandwiching the buffer between the slide and a microscope coverslip, as we described previously.[1, 5, 11, 14] Plasmonic images and LSPR spectra of single SMNOBS bound with single streptavidin molecules on the slide were imaged using DFOMS.

Stacks of the plasmonic images of single AgMMUA-Biotin-Streptavidin NPs were acquired from 420 to 720 nm at each nm (1 nm spectral resolution) with 100-ms exposure time using MSIS. The LSPR spectra of AgMMUA-Biotin-Streptavidin NPs were deconvoluted using individual LSPR spectrum of single AgMMUA-Biotin NPs via Cauchy-Lorentz distribution model (Figs. 3C, S4C, S6C), as described above. We then used PSF to determine the centroids (precise locations) of individual SMNOBS bound with single streptavidin molecules (Figs. 3D, S4D, S6D).

The processes were repeated twenty times for each binding complex (AgMMUA-Biotin-Streptavidin NPs) to generate the distribution of centroids of single SMNOBS in the complex (Figs. 4A, S5A, S7A). We then utilized 2D Gaussian to fit the distribution of centroids of each SMNOBS and to determine its precise locations at nm resolution (Figs. 4B-C, S5B, S7B), as described in SI.

We assembled the precise locations of single SMNOBS bound with single streptavidin molecules into super-resolution images at nm resolution (Figs. 4B-C, S5C, S7C). LSPR spectra of single SMNOBS bound with single streptavidin molecules at given precise positions determined using PHOTON were acquired to validate that their sum matched with the LSPR spectra of single AgMMUA-Biotin-Streptavidin NPs (Figs. 4D, S5D, S7D). Spatial and temporal resolutions of PHOTON were determined, as described in the text.

Electronic Supplementary Material (ESI) for Nanoscale
This journal is © The Royal Society of Chemistry 2011

TEM samples with the same molar ratio of streptavidin to SMNOBS at 10 were prepared and imaged using HRTEM (JEOL JEM-2100F).

Data Analysis and Statistics

We characterized 100 of single NPs (Ag, AgMMUA, AgMMUA-Biotin NPs) for each measurement of sizes and shapes of single Ag NPs using HRTEM, and plasmonic images and LSPR spectra of single Ag, AgMMUA, AgMMUA-Biotin NPs using DFOMS, to gain sufficient statistics to determine their size distribution and LSPR spectra (color) distribution that represent NP suspension in bulk solution at the single NP level. More than 100 of single AgMMUA-Biotin-Streptavidin NPs were imaged using PHOTON and HRTEM to gain sufficient statistics for mapping locations of single SMNOBS and their binding sites in single streptavidin molecules. Three measurements were performed for each experiment.

Electronic Supplementary Material (ESI) for Nanoscale
This journal is © The Royal Society of Chemistry 2011

B. Supplementary Figures and Figure Captions

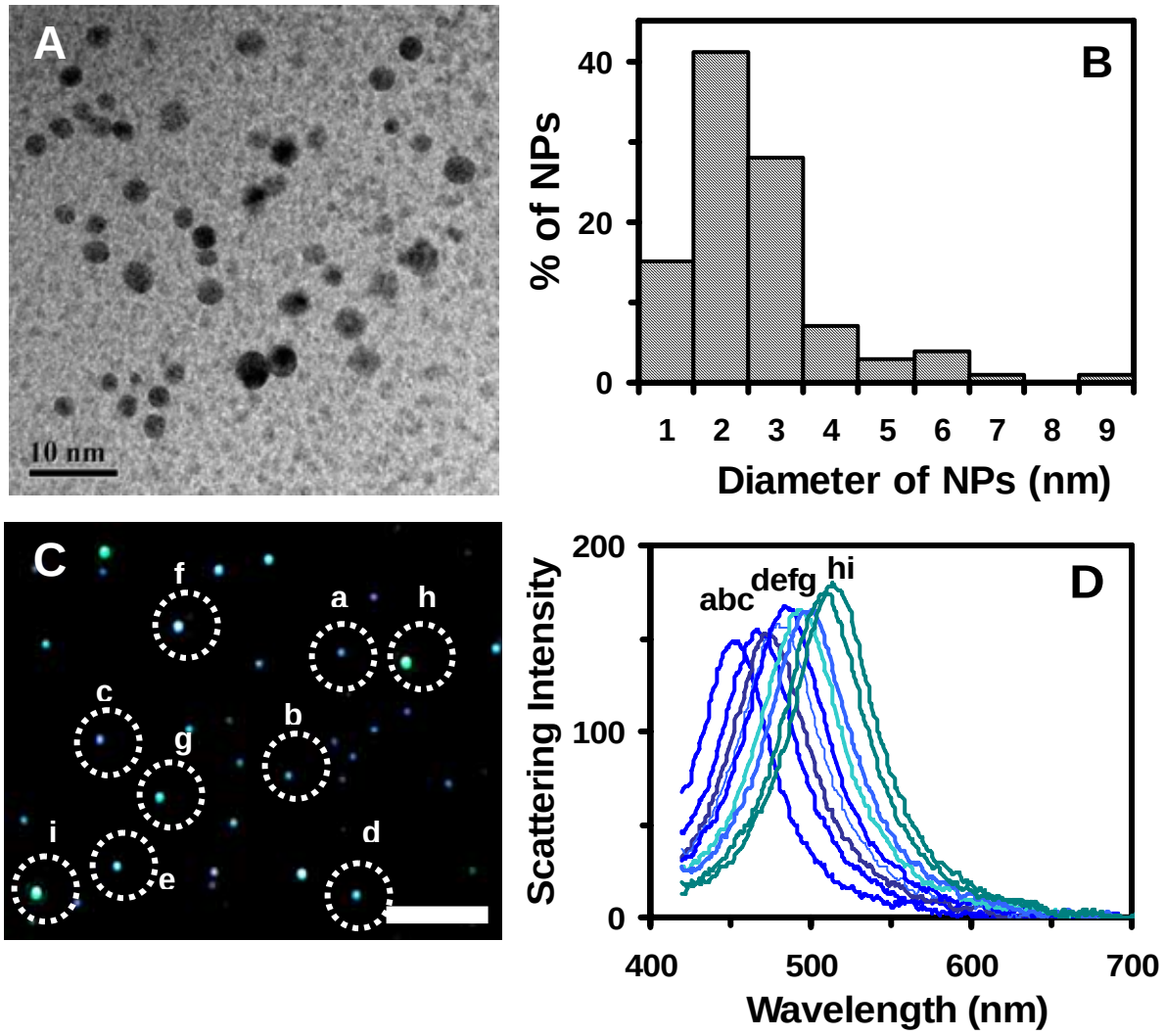


Fig. S1: Characterization of sizes and plasmonic optical properties of single Ag NPs: **(A)** HRTEM image of single Ag NPs and **(B)** Histogram of size distribution of single NPs show nearly spherical shape of NPs with average diameters of 2.6 ± 1.1 nm. **(C)** Dark field optical image and **(D)** LSPR spectra of single NPs show plasmonic blue and cyanic NPs with λ_{max} (FWHM) at (a) 450 (56), (b) 465 (60), (c) 472 (62), (d) 478 (64), (e) 482 (64), (f) 491 (64), (g) 496 (66), (h) 506 (64), and (i) 511 (65) nm, as circled in (C). Scale bars in (A) and (C) are 10 nm and 5 μm, respectively. The scale bar in (C) shows the distances between single NPs, but not the sizes of single NPs, because they are imaged under optical diffraction limit.

Electronic Supplementary Material (ESI) for Nanoscale
This journal is © The Royal Society of Chemistry 2011

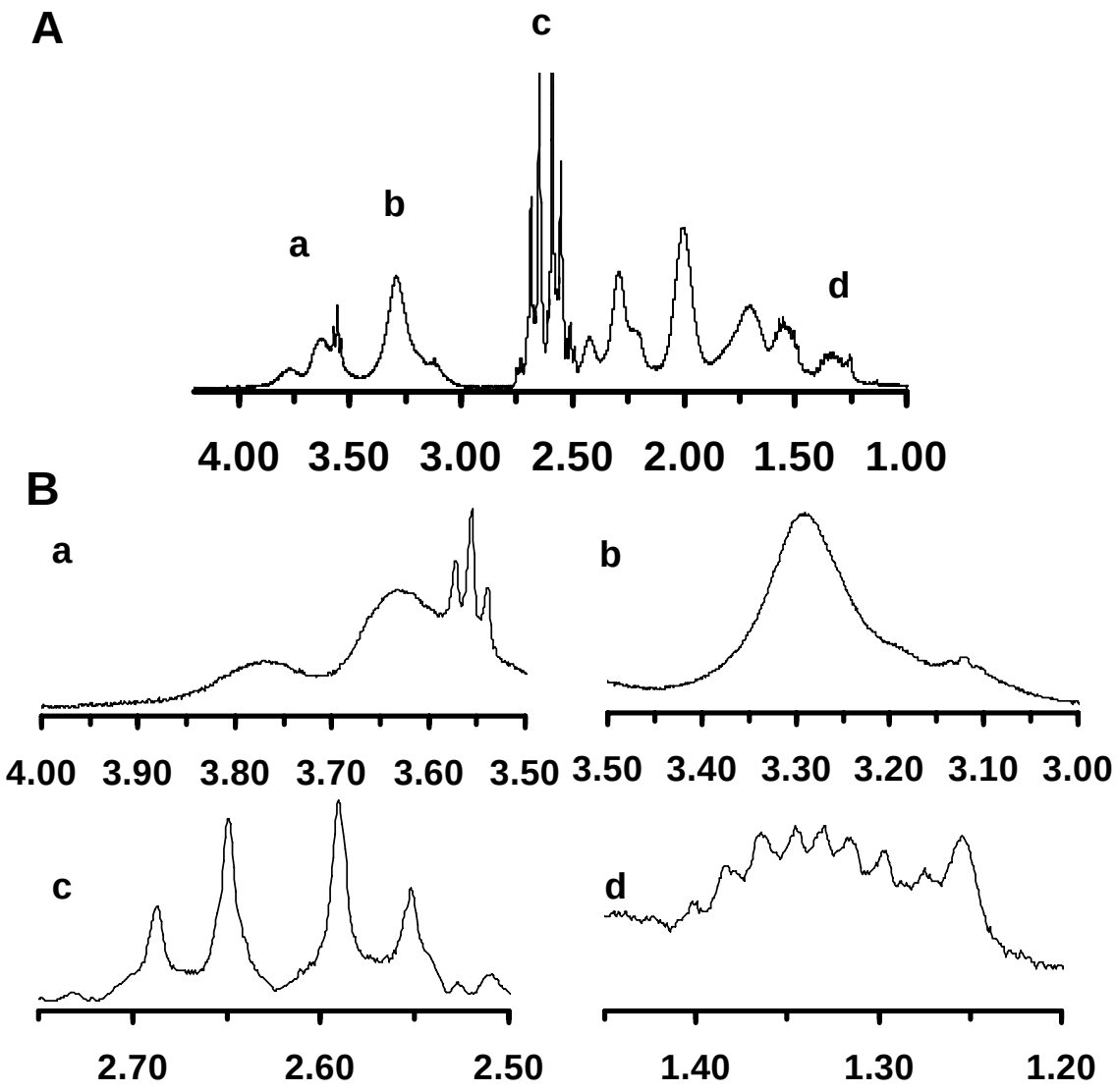


Fig. S2: NMR characterization of functional groups (citrate, MUA, MCH, PVP) attached on the surface of Ag NPs. **(A)** NMR spectra of AgMMUA NPs; **(B)** zoom-in individual peaks of NMR spectra in (A): (a) δ = 3.55 ppm, integration = 2.10, (**2H** in -(CH_2)-OH of MCH); (b) δ = 3.28 ppm, integration = 8.85, (**2H** from PVP ring); (c) δ = 2.62 ppm, integration = 28.03, (-C**H-**$_2$- next to thiol from both MUA and MCH and **4H** from citrate; (d) δ = 1.20-1.45 ppm, integration = 5.87, (**12H** from –$(CH_2)_2$-CH_2OH of MCH). Molar ratio of citrate : MCH : MUA : PVP = 33 : 5 : 1 : 0.03, showing a single carboxyl group per NP, as determined via a close-packing model.[1]

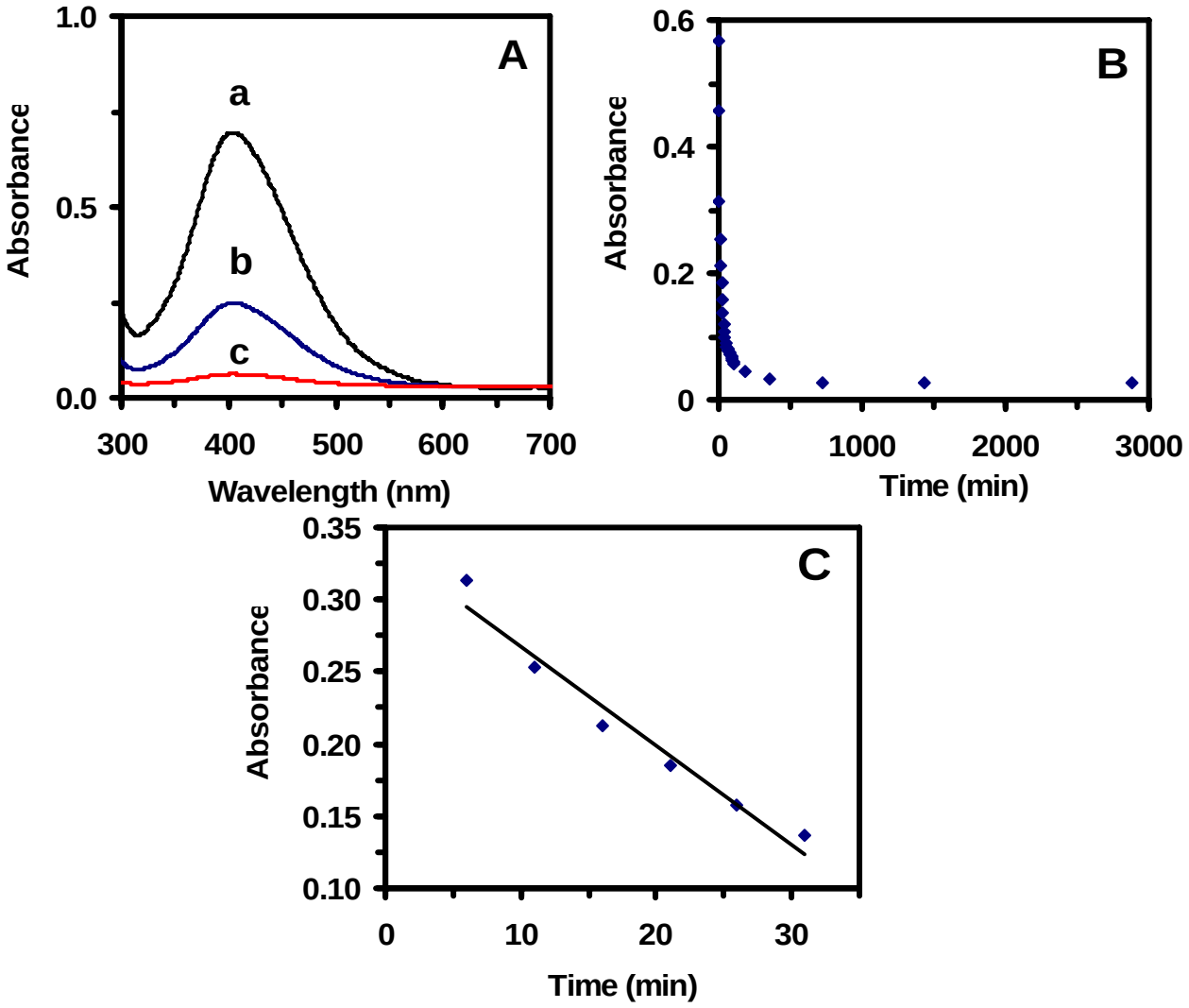


Fig. S3: Characterization of binding affinity and binding kinetics of AgMMUA-Biotin NPs (SMNOBS) with streptavidin: **(A)** UV-vis absorption spectra of 60 nM AgMMUA-Biotin NPs incubated with 600 nM streptavidin in PBS buffer (10 mM, pH 7.4) at (a) 0, (b) 21 min, and (c) 24 h, show that absorption peak wavelength at 403 ± 1 nm remains essentially unchanged, while the absorbance decreases with incubation time, suggesting that AgMMUA-Biotin NPs bound with streptavidin. **(B)** Plot of the peak absorbance corrected by baseline in (A) versus the incubation time, shows the exponential decay. **(C)** Zoom-in plot of (B) during 0 to 31 min, shows linearity with a slop of -6.8 x 10^{-3} min^{-1} and linear regression coefficient of determination (R^2) of 0.96. Binding constant ($3.2x10^{15}$) and associate rate constant ($6x10^2$ M^{-1} s^{-1}) are calculated using the approaches as we described previously.[1, 11]

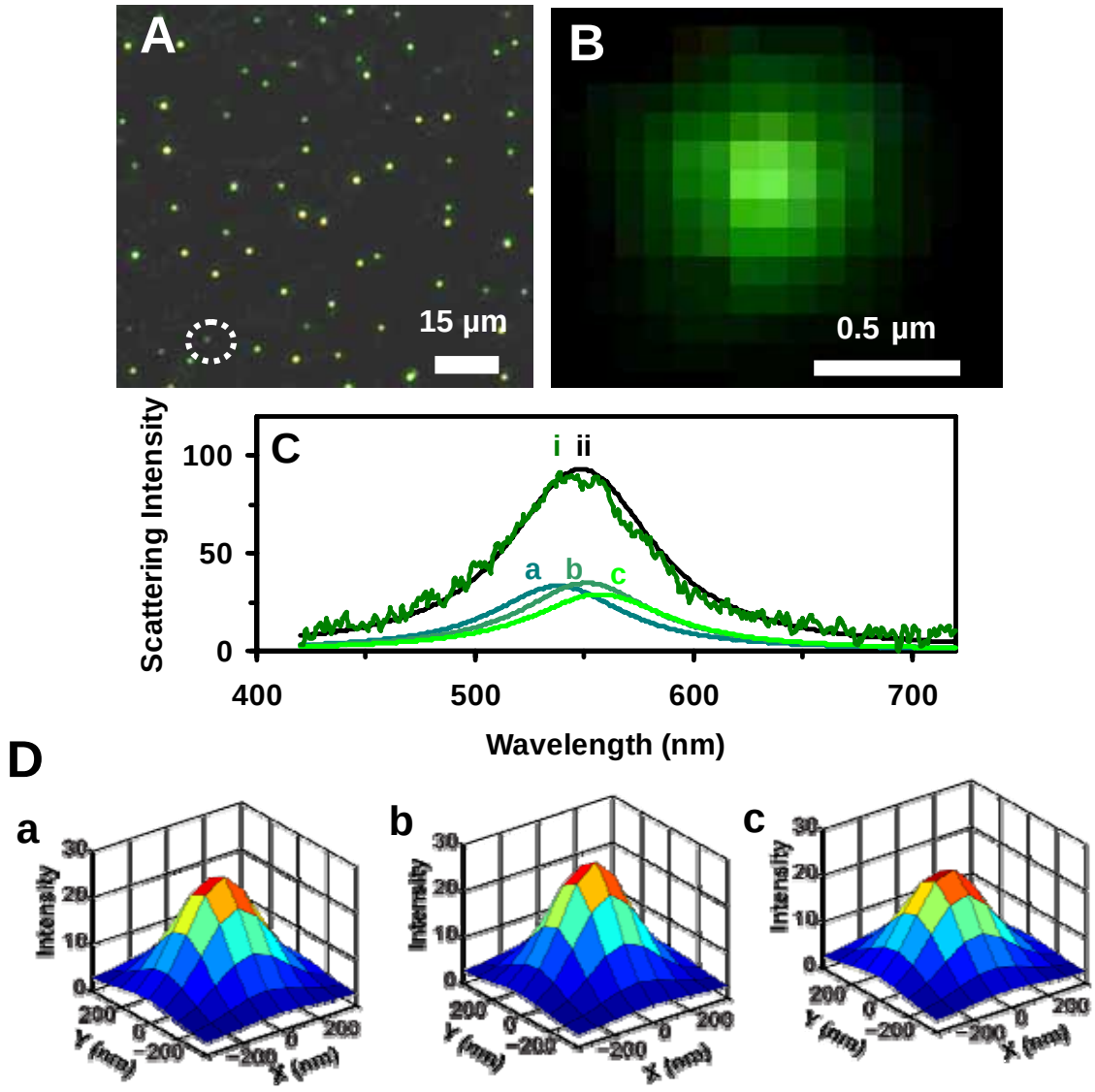


Fig. S4: Mapping of centroids of three SMNOBS bound with single streptavidin molecules using deconvolution and PSF. **(A)** Dark-field optical images of single AgMMUA-Biotin-Streptavidin NPs. **(B)** Zoom-in image of the NPs, circled in (A). **(C)**: (i) LSPR spectrum of the NPs in (B); (a-c) deconvoluted LSPR spectra of the spectrum in (i); and (ii) sum of deconvoluted LSPR spectra of (a-c), show λ_{max} (FWHM) at: (i) 547 (78); (ii) 548 (78); (a) 538 (68); (b) 551 (71); (c) 557 (66) nm. **(D)** Plots of scattering intensity of single SMNOBS with deconvoluted LSPR spectra of (a-c) in (C) versus their locations, respectively. As determined by PSF, the precise locations (centroids) of single AgMMUA-Biotin NPs bound with a streptavidin in (a-c) are (46.0, 64.0), (53.1, 59.2), (51.2, 51.2) nm, respectively. Scale bar in (A) and (B) are 15 and 0.5 μm, showing the distances between single NPs, but not the sizes of single NPs, due to optical diffraction limit.

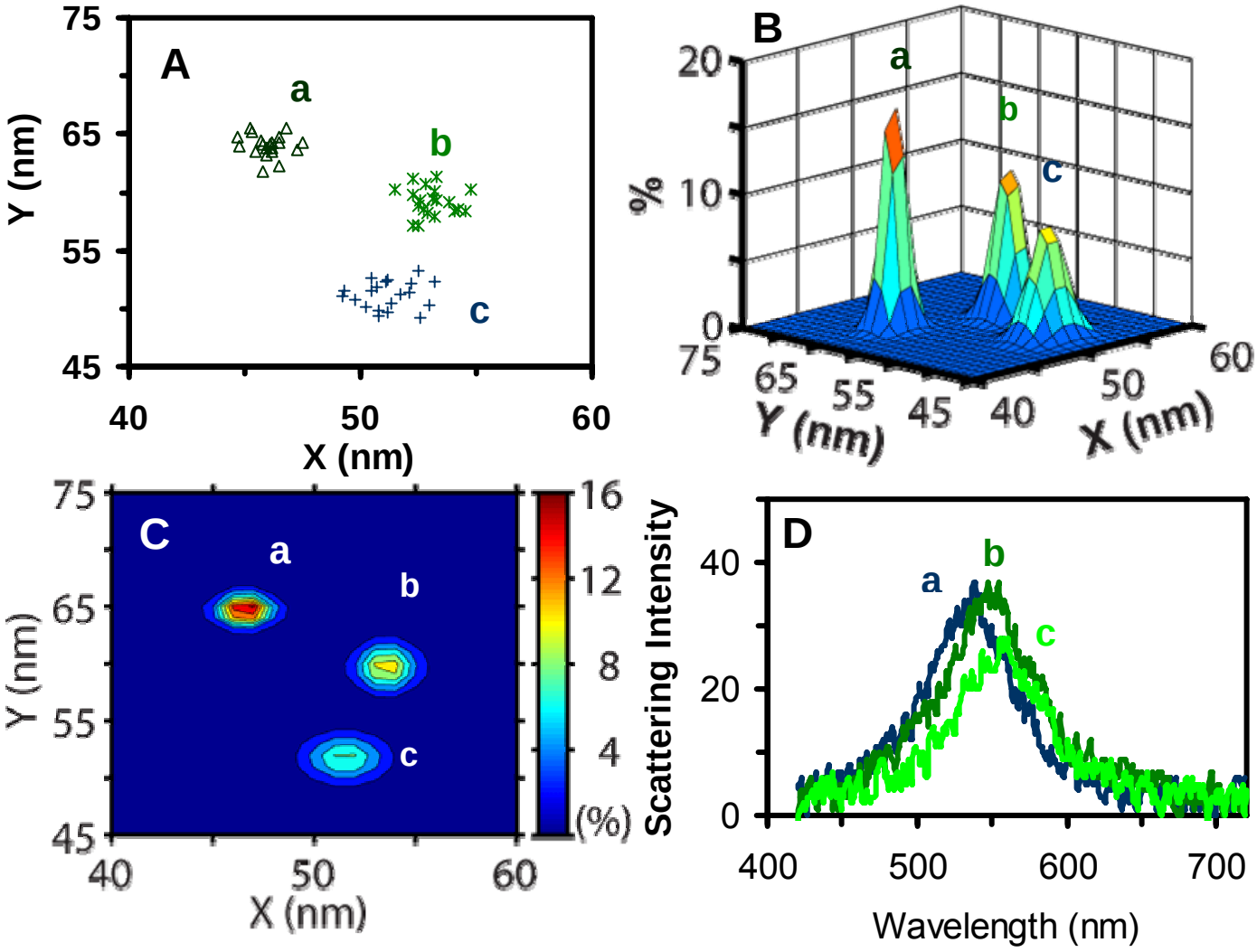


Fig. S5: Nanometer-resolution imaging of three SMNOBS bound with single streptavidin molecules (biotin-streptavidin complexes) using PHOTON. **(A)** Plots of distributions of precise locations (centroids) of single SMNOBS bound with a streptavidin molecule determined by PSF. Twenty repeated such measurements (points) are made for each NP. **(B)** 2D Gaussian fitting of the distributions of 20 precise locations of each NP in (A). **(C)** Contour plots of (B) show that centroids of single SMNOBS in (a-c) locate: at (46.0 ± 0.7, 64.0 ± 0.9); (52.1 ± 0.8, 59.2 ± 1.2); and (51.2 ± 1.1, 51.2 ± 1.2) nm, respectively. **(D)** LSPR spectra of single SMNOBS on the locations in (C) show λ_{max} (FWHM) at: (a) 538 (68); (b) 551 (71); and (c) 557 (66) nm, which agrees with deconvoluted LSPR spectra of single SMNOBS in Fig. S4C: a-c, respectively. Scale bar in (A) and (B) are 15 and 0.5 μm, showing the distances between single NPs, but not the sizes of single NPs, due to optical diffraction limit.

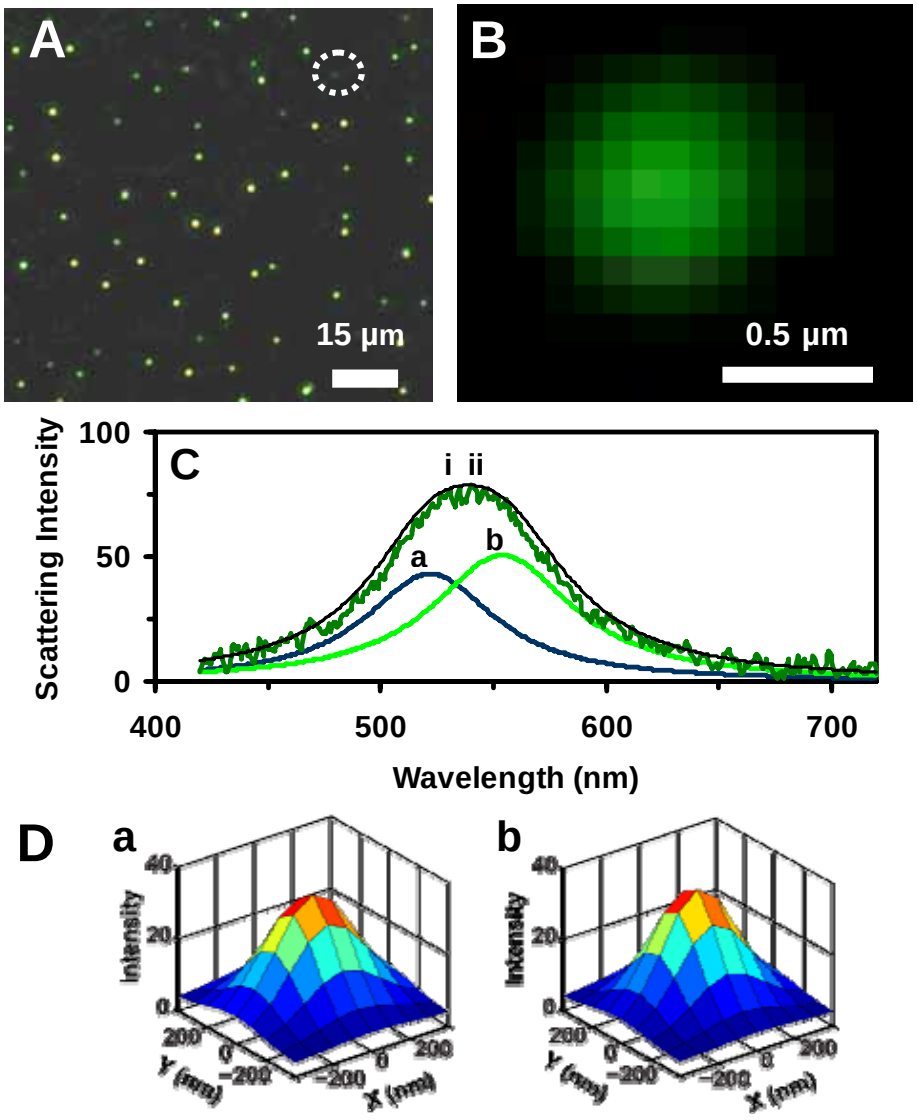


Fig. S6: Mapping of centroids of two SMNOBS bound with single streptavidin molecules using deconvolution and PSF. **(A)** Dark-field optical images of single AgMMUA-Biotin-Streptavidin NPs. **(B)** Zoom-in image of the NPs, circled in (A). **(C)**: (i) LSPR spectrum of the NPs in (B); (a-b) deconvoluted LSPR spectra of the spectrum in (i); and (ii) sum of deconvoluted LSPR spectra of (a-b), show λ_{max} (FWHM) at: (i) 540 (82); (ii) 540 (86); (a) 522 (62); (b) 554 (66) nm. **(D)** Plots of scattering intensity of single SMNOBS with deconvoluted LSPR spectra of (a-b) in (C) versus their locations, respectively. As determined by PSF, the precise locations (centroids) of single SMNOBS bound with a streptavidin in (a-b) are (41.9, 51.3), (45.0, 59.2) nm, respectively. Scale bar in (A) and (B) are 15 and 0.5 μm, showing the distances between single NPs, but not the sizes of single NPs, due to optical diffraction limit.

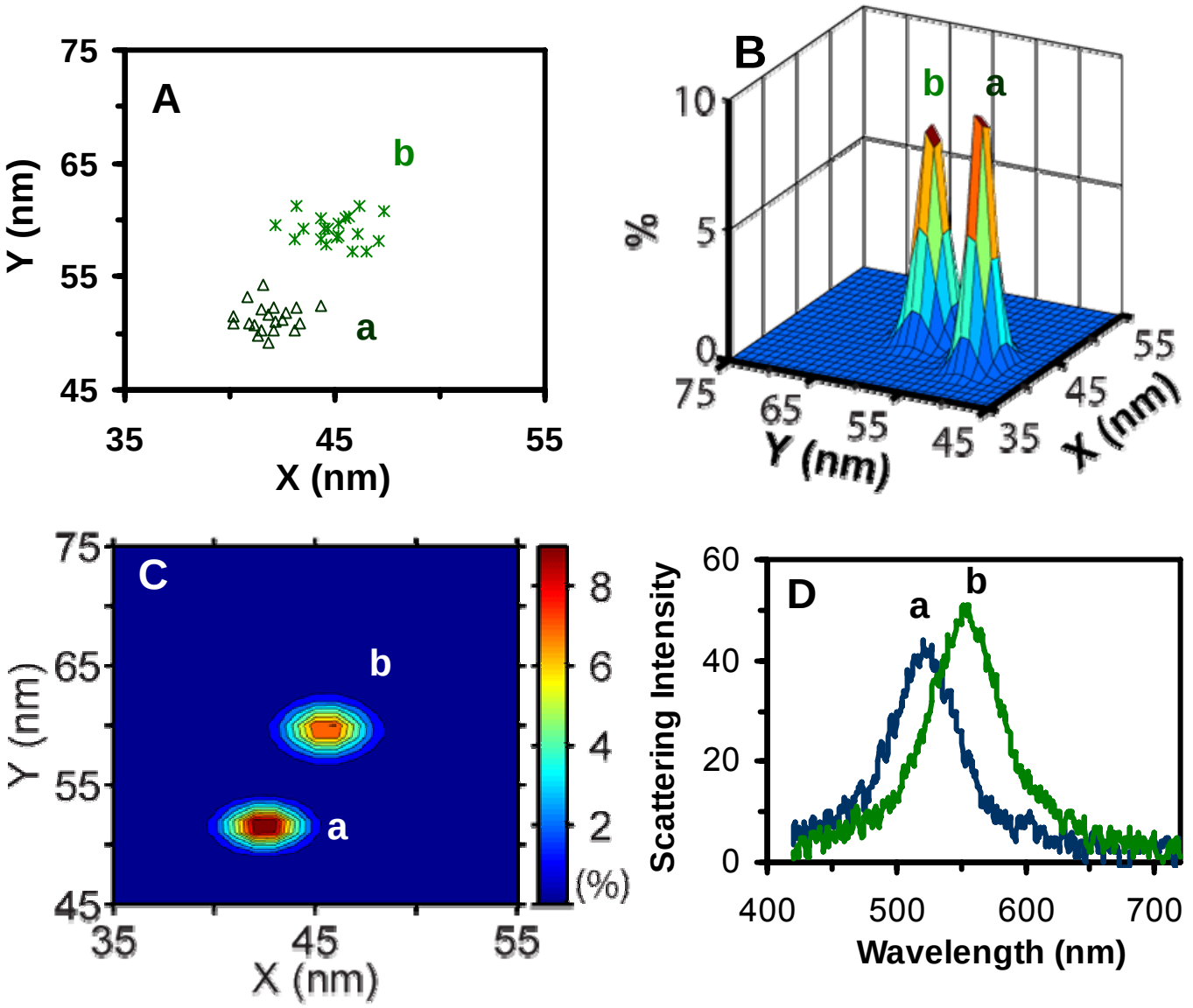


Fig. S7: Nanometer-resolution imaging of two SMNOBS bound with single streptavidin molecules (biotin-streptavidin complexes) using PHOTON. **(A)** Plots of distributions of centroids of single SMNOBS bound with a streptavidin molecule determined by PSF. Twenty repeated such measurements (points) are made for each NP. **(B)** 2D Gaussian fitting of the distributions of 20 precise locations of each SMNOBS in (A). **(C)** Contour plots of (B) show that centroids of single SMNOBS in (a-b) locate: at (41.9 ± 1.1, 51.3 ± 1.2) and (45.0 ± 1.3, 59.2 ± 1.2) nm, respectively. **(D)** LSPR spectra of single SMNOBS on the locations in (C) show λ_{max} (FWHM) at: (a) 522 (62) and (b) 554 (66) nm, which agrees with deconvoluted LSPR spectra of single SMNOBS in Fig. S6C: a-b, respectively.

Electronic Supplementary Material (ESI) for Nanoscale
This journal is © The Royal Society of Chemistry 2011

References

1. T. Huang, P. D. Nallathamby and X.-H. N. Xu, *J. Am. Chem. Soc.* , 2008, **130**, 17095-17105.
2. T. Huang and X.-H. N. Xu, *J. Mater. Chem.* , 2010, **20**, 9867-9876
3. K. J. Lee, P. D. Nallathamby, L. M. Browning, C. J. Osgood and X.-H. N. Xu, *ACS Nano*, 2007, **1**, 133-143.
4. X.-H. N. Xu, S. Huang, W. Brownlow, K. Salatia and R. Jeffers, *J. Phys. Chem. B.* , 2004, **108**, 15543-15551.
5. P. D. Nallathamby, K. J. Lee, T. Desai and X.-H. N. Xu, *Biochemistry*, 2010, **49**, 5942-5953.
6. P. D. Nallathamby and X.-H. N. Xu, *Nanoscale*, 2010, **2**, 942-952.
7. X.-H. N. Xu, W. J. Brownlow, S. V. Kyriacou, Q. Wan and J. J. Viola, *Biochemistry*, 2004, **43**, 10400-10413.
8. L. M. Browning, K. J. Lee, T. Huang, P. D. Nallathamby, J. Lowman and X.-H. N. Xu, *Nanoscale*, 2009, **1**, 138-152.
9. P. D. Nallathamby, K. J. Lee and X.-H. N. Xu, *ACS Nano*, 2008, **2**, 1371-1380.
10. Y. Song, P. D. Nallathamby, T. Huang, H. Elsayled-Ali and X.-H. N. Xu, *J. Phys. Chem. C.*, 2010, **114**, 74-81.
11. T. Huang, P. D. Nallathamby, D. Gillet and X.-H. N. Xu, *Anal. Chem.*, 2007, **79**, 7708-7718.
12. S. V. Kyriacou, W. J. Brownlow and X. H. N. Xu, *Biochemistry*, 2004, **43**, 140-147.
13. S. V. Kyriacou, M. E. Nowak, W. J. Brownlow and X.-H. N. Xu, *J. Biomed. Opt.*, 2002, **7**, 576-586.
14. X.-H. N. Xu, J. Chen, R. B. Jeffers and S. V. Kyriacou, *Nano Lett.*, 2002, **2**, 175-182.
15. X.-H. N. Xu and R. P. Patel, in *Encyclopedia of Nanoscience and Nanotechnology*, ed. H. S. Nalwa, American Scientific Publishers, Stevenson Ranch, CA, 2004, vol. 7, pp. 189-192.
16. X.-H. N. Xu, Y. Song and P. D. Nallathamby, in *New Frontiers in Ultrasensitive Bioanalysis: Advanced Analytical Chemistry Applications in Nanobiotechnology, Single Molecule Detection, and Single Cell Analysis*, ed. X.-H. N. Xu, Wiley, New Jersey, 2007, pp. 41-65.
17. S. C. Gebhart, R. C. Thompson and A. Mahadevan-Jansen, *Appl. Opt.*, 2007, **46**, 1896-1910.
18. M. Gonzalez, L. A. Bagatolli, I. Echabe, J. L. R. Arrondo, C. E. Argarana, C. R. Cantor and G. D. Fidelio, *J. Biol. Chem.*, 1997, **272**, 11288-11294.
19. O. H. Laitinen, V. P. Hytönen, H. R. Nordlund and M. S. Kulomaa, *Cell Mol. Life Sci.* , 2006, **63**, 2992-3017.
20. W. A. Hendrickson, A. Pähler, J. L. Smith, Y. Satow, E. A. Merritt and R. P. Phizackerley, *Proc. Natl. Acad. Sci. U. S. A.* , 1989, **86**, 2190-2194.
21. A. Delaigle, P. Hall and A. Meister, *Ann Stat.* , 2008, **36**, 665-685.
22. R. D. B. Fraser and E. Suzuki, *Anal. Chem.*, 1969, **41**, 37-39.
23. T. Klar, M. Perner, S. Grosse, G. von Plessen, W. Spirkl and J. Feldmann, *Phys. Rev. Lett.*, 1998, **80**, 4249-4252.
24. V. D. Barnett, *J. Amer. Statist. Assoc.*, 1966, **61**, 1205-1218.
25. D. L. Farkas, C. Du, G. W. Fisher, C. Lau, W. Niu, E. S. Wachman and R. M. Levenson, *Comp. Med. Imag. Graph.*, 1998, **22**, 89-102.
26. R. E. Thompson, D. R. Larson and W. W. Webb, *Biophys. J.*, 2002, **82**, 2775-2783.